ChemPubSoc Europe

DOI: 10.1002/cmdc.201400049

Gold(I) Biscarbene Complexes Derived from Vascular-Disrupting Combretastatin A-4 Address Different Targets and Show Antimetastatic Potential

Julienne K. Muenzner,[a] Bernhard Biersack,[a] Hussein Kalie,[a] Ion C. Andronache,[b] Leonard Kaps,[c] Detlef Schuppan,[c] Florenz Sasse,[d] and Rainer Schobert*[a]

Gold *N*-heterocyclic carbene (NHC) complexes are an emerging class of anticancer drugs. We present a series of gold(I) biscarbene complexes with NHC ligands derived from the plant metabolite combretastatin A-4 (CA-4) that retain its vascular-disrupting effect, yet address different cellular and protein targets. Unlike CA-4, these complexes did not interfere with tubulin, but with the actin cytoskeleton of endothelial and cancer cells. For the highly metastatic 518A2 melanoma cell line this effect was accompanied by a marked accumulation of cells in the G_1 phase of the cell cycle and a suppression of active prometastatic matrix metalloproteinase-2. Despite these mechanistic differences the complexes were as strongly antivascular as CA-4 both in vitro in tube formation assays with human umbilical vein endothelial cells, and in vivo as to blood vessel disruption in the chorioallantoic membrane of chicken eggs. The antiproliferative effect of the new gold biscarbene complexes in a panel of six human cancer cell lines was impressive, with low sub-micromolar IC_{50} values (72 h) even against CA-4-refractory HT-29 colon and multidrug-resistant MCF-7 breast carcinoma cells. In preliminary studies with a mouse melanoma xenograft model the complexes led to significant decreases in tumor volume while being very well tolerated.

Introduction

Tumor blood vessels, which are physiologically different from normal vasculature, are a promising pharmacological target that can be addressed in two different ways.[1–3] While antiangiogenic therapies aim to impede the development of new blood vessels by interference with angiogenic signaling pathways, vascular-disrupting agents (VDA) destroy existing disorganized tumor blood vessels.[4] The *cis*-stilbene combretastatin A-4 (CA-4, **1a**) is a VDA that was first isolated from the bark of the South African Cape Bushwillow (*Combretum caffrum*).[5] It induces a rapid vascular shutdown in solid tumors, eventually leading to secondary tumor cell death.[6] The antitumor activity of **1a** originates from two different modes of action. It binds strongly to the colchicine binding site of tubulin, resulting in destabilization of the microtubule cytoskeleton and inhibition of mitosis,[7] and it interferes with the VE-cadherin/β-catenin/Akt signaling pathway in vascular endothelial cells, which is crucial for cell migration and adhesion.[8] Fosbretabulin (CA-4P, **1b**), a phosphate prodrug of **1a** with improved bioavailability, has demonstrated its selectivity for tumor vasculature in a number of clinical trials.[7,9] However, due to its insufficient cytotoxicity, **1b** must be administered in combination with other anticancer drugs such as carboplatin or bevacizumab to prevent revascularization of persistent cancer cell colonies and a relapse of the disease.[10,11] One reason for the insufficient anticancer activity of **1a** is its propensity to isomerize into a biologically inactive *E*-alkene isomer.[12,13] This can be prevented by incorporation of the *Z*-alkene in heterocycles such as imidazoles, triazoles, or oxazoles.[7,14,15] We previously reported new, chemically stable *N*-methyl-4,5-diarylimidazole analogues of **1a** that showed a synergism of vascular disruption and enhanced cytotoxic effects.[16] They also bind tightly to tubulin, interfere with microtubule formation, and seem to operate by a mechanism akin to that of **1a** with the distinction of being chemically stable, water soluble, and selective for malignant cells, even those resistant to **1a**. Some imidazolium salts also proved efficacious against chemoresistant tumor xenografts in mice.[16]

Imidazoles also happen to be a prominent ligand type in *N*-heterocyclic carbene (NHC) complexes of late transition metals which have been used thus far mainly as robust catalysts for organic synthesis. Recently, imidazol-2-ylidene complexes of silver and gold have been studied as potential anticancer drugs with a focus on metal interactions with DNA and apoptosis-relevant proteins.[17,18] The aspect of a suitably substituted imidazole contributing some antivascular effect to the overall activity profile of such NHC complexes has been largely

[a] *J. K. Muenzner, Dr. B. Biersack, H. Kalie, Prof. Dr. R. Schobert*
Department of Organic Chemistry, University Bayreuth
Universitätsstraße 30, 95440 Bayreuth (Germany)
E-mail: Rainer.Schobert@uni-bayreuth.de

[b] *Dr. I. C. Andronache*
Independent Researcher in Fractal Analysis and Medical Geography
Aleea Policlinicii 3, 810262 Braila (Romania)

[c] *L. Kaps, Prof. Dr. D. Schuppan*
Institute of Translational Immunology
University Medical Center of the Johannes Gutenberg University Mainz
Langenbeckstraße 1, 55131 Mainz (Germany)

[d] *Dr. F. Sasse*
Department of Chemical Biology, Helmholtz Centre for Infection Research
Inhoffenstraße 7, 38124 Braunschweig (Germany)

Supporting information for this article is available on the WWW under http://dx.doi.org/10.1002/cmdc.201400049.

neglected. To fill this gap, we synthesized and evaluated gold(I) carbene complexes derived from imidazoles that had been optimized for antivascular efficacy. We already reported on the cytotoxicity and the cellular uptake of a small series of such new gold(I) NHC complexes.[19,20] Gold complex **2**, bearing an imidazole with the privileged combretastatin substituents, exhibited both anticancer activity and pronounced antivascular effects in vitro and in vivo. Surprisingly, and in contrast to **1a** and the underlying imidazolium salts, these effects by complex **2** were not correlated to tubulin binding. Herein we present an in-depth study of the mechanism of action of a new series of analogous cationic gold(I) biscarbene complexes **10** and **11**.

Results and Discussion

Chemistry

The new gold(I) biscarbene complexes **10** and **11** were prepared by reaction of the imidazolium tetrafluoroborates **8** and **9** with Ag_2O to give the corresponding silver carbene complexes which were subsequently transmetalated with $AuCl(SMe_2)$ (Scheme 1). The salts **8** and **9** were obtained from reaction of the iodides **6** and **7** with $NaBF_4$, which in turn were available by N-alkylation of the imidazoles **4** and **5** with methyl iodide or ethyl iodide, respectively. These imidazoles were accessible by van Leusen reactions of TosMIC reagents **3**[19] with anisaldehyde and methyl- or ethylamine. We confined this study to complexes that bear identical residues on the nitrogen atoms and to variation in only one *meta* substituent on the A-ring, a position that had been found most crucial in previous tests with similar oxazoles and imidazoles.[16]

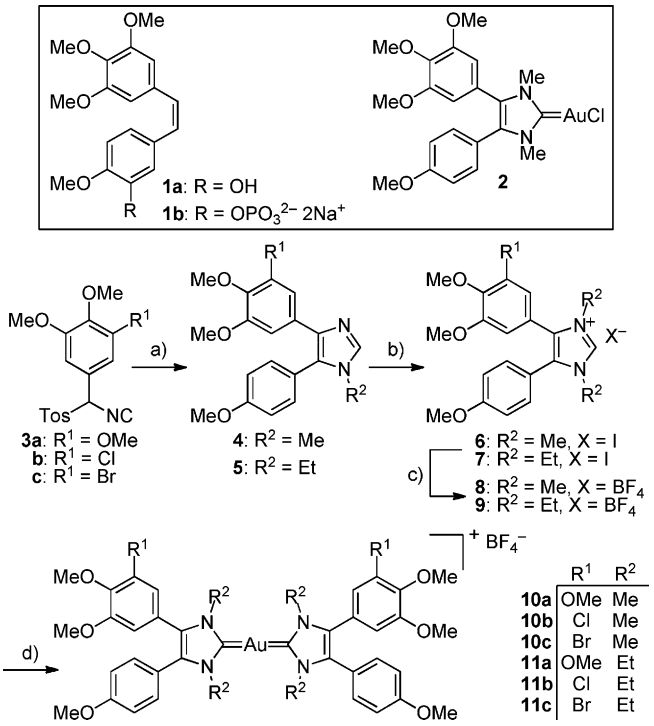

Scheme 1. Top box: structures of combretastatin A-4 (**1a**), fosbretabulin (**1b**), and the known complex **2**. Scheme: syntheses of complexes **10** and **11**. *Reagents and conditions*: a) anisaldehyde, $MeNH_2$/EtOH or $EtNH_2$/THF, AcOH, EtOH, reflux, 2 h, then **3**, K_2CO_3, reflux, 3 h; b) MeI or EtI, MeCN, 80 °C, 16 h; c) $NaBF_4$, acetone, RT, 24 h; d) Ag_2O (1 equiv), CH_2Cl_2, RT, 5 h, then $AuCl(SMe_2)$ (0.5 equiv), CH_2Cl_2, RT, 16 h, 82% (**10a**), 81% (**10b**), 80% (**10c**), 40% (**11a**), 75% (**11b**), 77% (**11c**).

Growth inhibition assay

The inhibitory effect of complexes **10** and **11** on the growth of cancer cells was evaluated with 3-(4,5-dimethylthiazol-2-yl)-2,5-diphenyltetrazolium bromide (MTT) to identify viable cells that reduce it to a violet formazan.[21] The biscarbene complexes **10** and **11** showed distinct antiproliferative effects against a panel of six cancer cell lines of five different entities with IC_{50} values (72 h) mostly in the low submicromolar range (Table 1). Figure 1 depicts their cell-line specificities, that is, their IC_{50} values against individual cell lines with respect to the mean IC_{50} value over all cell lines of the panel.

The all-methoxy-substituted complexes **10a** and **11a** showed their highest activity in HT-29 colon carcinoma cells, whereas the chloro derivatives **10b** and **11b** were most efficacious against the multidrug-resistant MCF-7 breast carcinoma cells. The bromo compounds **10c** and **11c** displayed little cell-line specificity. All complexes were least active ($IC_{50} > 1$ μM) against resistant cervical KB-V1 cells, which overexpress P-glycoprotein (P-gp) type ABC transporters.[22,23] Interestingly, when these cells had been pretreated for 24 h with the P-gp substrate ve-

Table 1. Inhibitory concentrations of compounds **1a**, **10**, and **11** toward various cancer cell lines.

Cell line[a]	IC_{50} [μM][b]						
	1a[16]	**10a**	**10b**	**10c**	**11a**	**11b**	**11c**
518A2	0.02 ± 0.01	0.46 ± 0.02	0.31 ± 0.02	0.37 ± 0.02	0.43 ± 0.04	0.43 ± 0.04	0.23 ± 0.06
Panc-1	ND[c]	0.40 ± 0.07	0.16 ± 0.01	0.26 ± 0.00	0.19 ± 0.07	0.36 ± 0.04	0.18 ± 0.01
HCT-116	ND	0.30 ± 0.02	0.11 ± 0.00	0.11 ± 0.01	0.18 ± 0.02	0.07 ± 0.01	0.12 ± 0.00
HT-29	3.6 ± 0.1	0.08 ± 0.02	0.15 ± 0.01	0.13 ± 0.01	0.06 ± 0.01	0.10 ± 0.01	0.16 ± 0.01
MCF-7/Topo	0.50 ± 0.20	0.18 ± 0.04	0.06 ± 0.00	0.15 ± 0.06	0.08 ± 0.02	0.06 ± 0.01	0.10 ± 0.02
MCF-7/Topo + fumit. C	ND	0.19 ± 0.01	0.09 ± 0.01	0.12 ± 0.00	0.13 ± 0.01	0.08 ± 0.00	0.10 ± 0.01
KB-V1/Vbl	< 0.01	7.7 ± 0.3	2.0 ± 0.3	3.9 ± 0.5	3.7 ± 0.2	1.1 ± 0.1	1.5 ± 0.0
KB-V1/Vbl + verapamil	ND	2.9 ± 0.3	0.23 ± 0.03	0.45 ± 0.06	1.3 ± 0.1	0.22 ± 0.02	0.20 ± 0.05

[b] Human cancer cell lines: 518A2 melanoma, Panc-1 pancreatic ductular adenocarcinoma, HCT-116 and HT-29 colon carcinomas, MCF-7/Topo breast adenocarcinoma (optionally pretreated with 1.2 μM fumitremorgin C for 24 h), KB-V1/Vbl cervix carcinoma (optionally pretreated with 24 μM verapamil·HCl for 24 h). [b] Values are the means ± SD of four independent experiments and are derived from dose–response curves obtained by measuring the percentage of viable cells relative to untreated controls after 72 h incubation using the MTT assay. [c] ND: not determined.

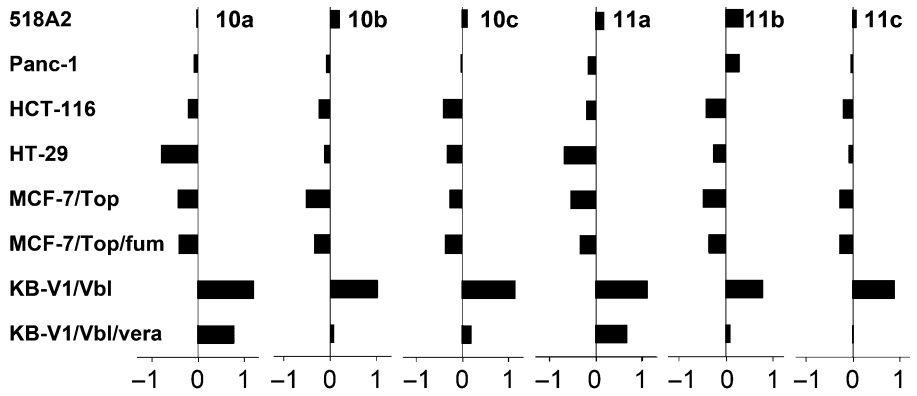

Figure 1. Cell line specificities of gold biscarbene complexes **10a**–**c** and **11a**–**c** as deviation of the log (IC_{50}/72 h) of individual cell lines from the mean over all cell line log (IC_{50}/72 h) values. Negative values indicate higher, positive values lower than average activities. Mean log (IC_{50}/72 h): −6.31 (**10a**), −6.71 (**10b**), −6.55 (**10c**), −6.54 (**11a**), −6.74 (**11b**), −6.70 (**11c**).

rapamil,[24,25] the activity of the halo-substituted complexes **10b**,**c** and **11b**,**c** rose five- to tenfold. In contrast, **10a** and **11a** profited far less from the addition of the competitor substrate verapamil. Apparently, their methoxy-only substituted ligands render them better substrates for the P-gp efflux pumps. Cells of the human breast carcinoma MCF-7/Topo, which overexpress ABC transporters of the breast cancer resistance protein (BCRP) type, responded fairly well to all complexes **10** and **11**. Pretreatment of these cells with fumitremorgin C, a selective BCRP inhibitor,[26] did not alter the IC_{50} values of the complexes much, which indicates that they are not substrates of this particular efflux pump. This fact is important because BCRP is also thought to be responsible for the drug resistance of certain cancer stem-like cells.[27]

Effects on cytoskeletal components

We previously showed that in contrast to **1a** and its imidazolium salt derivatives, the gold carbene complex **2** does not interfere with the polymerization of purified tubulin in vitro.[19] We now subjected the corresponding biscarbene complex **10a** to the same fluorescence-based tubulin polymerization assay and found that it also does not affect the polymerization of purified tubulin (Supporting Information, Figure S1). Next, we looked for effects of compounds **10** and **11** on the cytoskeletal organization of microtubules and microfilaments (F-actin) in 518A2 melanoma cells and in non-malignant human umbilical vein endothelial cells (HUVEC). As anticipated, the distribution of microtubules in both types of cells treated with **10** or **11** for 24 h did not appear different from untreated controls when visualized by immunofluorescence (Supporting Information, Figure S2). In contrast, exposure to **1a** led to a massive destruction of the microtubule cytoskeleton in both cell lines (Supporting Information, Figure S2). Exposure of both cell lines to **10** and **11** for 24 h triggered a complete reorganization of the actin cytoskeleton with formation of stress fibers stretched across the whole cell body, which is a typical cell response to chemical or physical stress (Figure 2). In contrast to **1a**, the gold complexes **10** and **11** induced stress fiber formation without concomitant destruction of the microtubule cytoskeleton.[28] The untreated control cells of either type showed the typical cortical microfilaments with only few fine filaments traversing the cells as well as a greater number of intercellular connections.[28,29]

Cell-cycle analysis

The antimitotic effect of **1a** is based on microtubule disruption and stress fiber formation leading to G_2/M-phase cell-cycle arrest.[30,31] Because the new gold complexes mediated the formation of stress fibers without affecting microtubules, we investigated whether they also alter cell-cycle progression in 518A2 melanoma cells (Figure 3). 518A2 cells accumulated in the G_1 phase when exposed to compounds **10** or **11** for 24 h, while the sub-G_1 population of apoptotic cells was barely increased, which means there is a clear correlation between stress fiber formation and the G_1 phase arrest.

Wound healing assay

The effects of complexes **10** and **11** on the motility of cancer cells were analyzed by introducing an artificial "scratch wound" to monolayers of 518A2 melanoma cells and monitoring the closure of this gap over time. While control cells overgrew the 'wound' within 48 h (100% of wound healing), it took much longer for 518A2 cells treated with complexes **10** or **11** (Figure 4; for exemplary light microscopy images see Supporting Information, Figure S3). The *N*-ethyl complexes **11** were generally more effective than their corresponding *N*-methyl analogues **10**, inhibiting the wound healing to the same extent as **1a** (IC_{50} = 20 nM)[16] after 48 h incubation with equitoxic concentrations. Because a functional, dynamic actin cytoskeleton is essential for cell migration, the antimigratory activity of gold complexes **10** and **11** is likely to be a consequence of their induction of stress fibers[32,33] and of G_1 phase arrest of the 518A2 cell cycle.

Effects on matrix metalloproteinases

Tumor angiogenesis and metastasis require degradation of the basement membrane so that endothelial or tumor cells may migrate through the extracellular matrix (ECM) and egress from or invade tissues.[34] This proteolytic degradation of ECM components is mediated by matrix metalloproteinases (MMPs), a class of zinc-dependent endopeptidases that are expressed and secreted at elevated concentrations by inflammatory, fibroblastic, and especially vascular endothelial cells and invasive tumor cells.[35] Because of their essential role in tumor progression, MMPs were earmarked as promising pharmacological an-

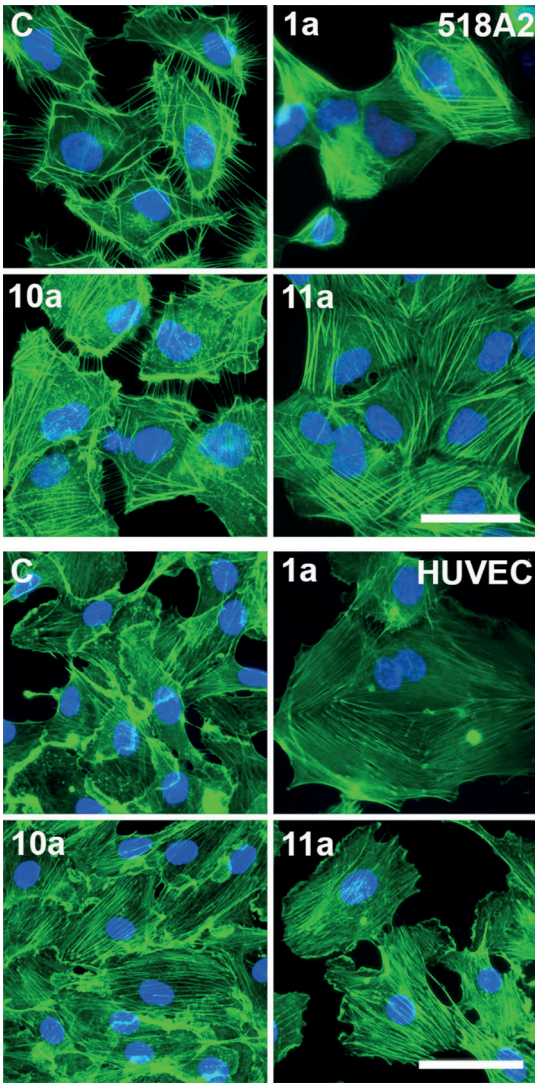

Figure 2. Effects on the cellular organization of microfilaments. The actin cytoskeleton of both cell types was visualized by labeling with an Alexa Fluor 488 phalloidin conjugate. Upper group of four images: 518A2 melanoma cells treated with vehicle (C, control), 2.5 nM **1a**, 250 nM **10a** or 500 nM **11a**. Lower group of four images: HUVEC treated with vehicle (C, control), 100 nM each of **1a** or **10a** and 1 μM **11a**. Scale bars: 50 μm; images are representative of two independent experiments.

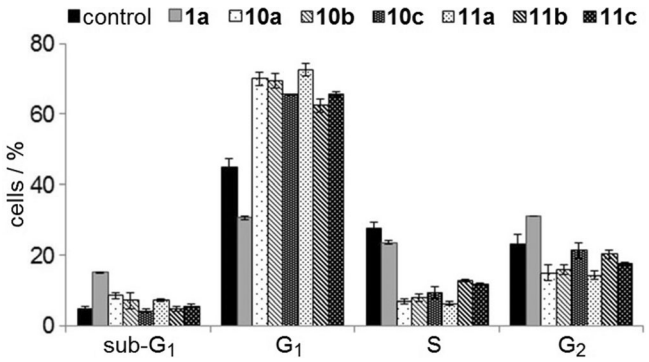

Figure 3. Effects of **1a** and complexes **10** and **11** on cell-cycle progression of 518A2 melanoma cells. Percentages are shown of cells in G_1, S, or G_2 phases as well as apoptotic cells (sub-G_1) as obtained by flow cytometry after DNA staining with propidium iodide. Cells were treated with 5 nM **1a** and 500 nM each of **10** or **11**. Values are the means ± SD of three independent experiments.

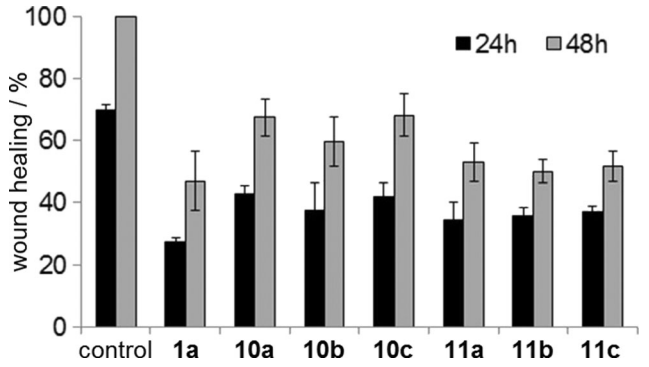

Figure 4. Inhibitory effects of **1a** and gold complexes **10** and **11** on the migration of 518A2 melanoma cells. Cells were treated with 5 nM **1a** or 500 nM **10** or **11**. Values are the means ± SD of three independent experiments.

ticancer targets. Notably, activity of the basement membrane collagen degrading MMP-2 and MMP-9 can be analyzed by zymography.[36] The monocarbene complex **2** was previously shown by us to only slightly affect the activities of MMP-2 and -9 in HUVEC, while a related gold(I) *N*,*N*-dibenzylimidazol-2-yl carbene complex significantly decreased the cell-associated and secreted levels of active MMP-2.[20] In this study we examined the effects of the biscarbene complexes **10** and **11** on the intra- and extracellular levels of active MMP-2 and -9 produced by 518A2 melanoma cells, via gelatin zymography (Figure 5).

The test compounds decreased the levels of active MMP-2, while the fractions of MMP-9 were left virtually unaltered. Moreover, the levels of active cell-associated MMP-2 (in cell lysates) were generally decreased to a greater extent than secreted MMP-2. Complex **11b** was the most active compound and depressed the levels of functional MMP-2 significantly, even at concentrations as low as 100 nM. To clarify whether complexes **10** and **11** actually do interfere with the expression or secretion of MMP-2 or rather inhibit metalloproteinase activity, we subjected pooled zymography protein samples from experiments with or without the most active complex **11b** to western blot analysis (Supporting Information, Figure S4). Because the levels of cell-associated and secreted MMP-2 protein were decreased by complex **11b**, it must have interfered with the expression or secretion of MMP-2 rather than by acting as a mere inhibitor of this particular matrix metalloproteinase.

In vitro and in vivo antivascular activity

The inhibitory effects of the new gold complexes on the ability of HUVEC to form tubular networks in vitro when seeded on thin layers of matrigel can be used as a predictor for their antivascular effects in vivo.[37] Hence, the in vitro antivascular activity of the all-methoxy-substituted gold complexes **10a** and **11a** was exemplarily investigated by tube-formation assay (Supporting information, Figure S5).[38] Control HUVEC devel-

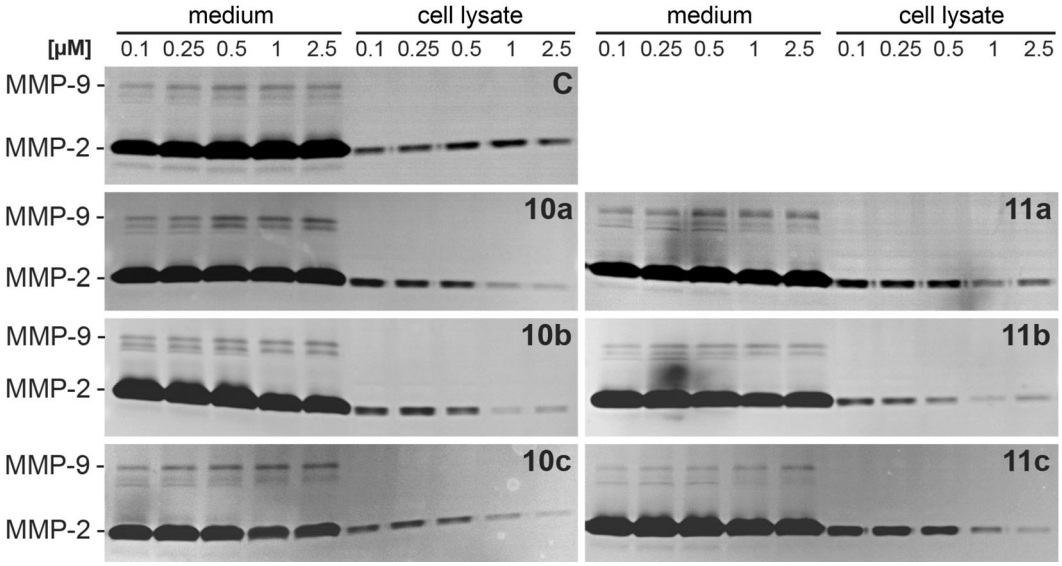

Figure 5. Effects of complexes **10** and **11** at 100 nM to 2.5 μM on the cell-associated and secreted activities of MMP-2 and -9 in 518A2 melanoma cells after 24 h exposure. Conditioned media and cell lysates were subjected to gelatin zymography. C: control (DMF); shown are negative images of the gelatin gels.

oped networks of interconnected tubes linked by well-defined branch points after 24 h growth on matrigel. Exposure of HUVEC to **10a** or **11a** for 24 h completely prevented the formation of organized tubular networks, so that only few sprouting points and fragmented tubules could be detected. Complex **11a** was found to be nearly as effective as the natural lead compound **1a**.

We then used the chorioallantoic membrane (CAM) assay as a model system to identify vascular-disruptive activities of the complexes in vivo.[39,40] Figure 6 shows such effects as detected for **1a** and the most active complexes, **10b** and **11a**. Such vascular-disrupting effects can be quantified by calculating the decrease in the area covered by blood vessels in CAM micrographs using vessel area analysis that is derived from fractal analysis.[41,42] Figure 7 shows a comparison of all complexes **10** and **11**. On average, the chloro-substituted complexes **10b** and **11b** were most strongly vascular-disruptive after 6 h exposure. The all-methoxy-substituted complex **10a** was slightly less effective, while the bromo derivatives **10c** and **11c** exhibited the weakest antivascular activity. The natural lead **1a** also showed strong disruptive effects, yet only when applied at higher concentrations than the gold complexes. Unlike in eggs treated with **1a**, the vasculature exposed to complexes **10** and **11** was able to partially recover and sprout new blood vessels within 24 h. Interestingly, monocarbene complex **2**, while leaving tube formation by HUVEC and migration of 518A2 melanoma cells virtually unaffected, led to a distinct and irreversible blood vessel disruption in the CAM assay.

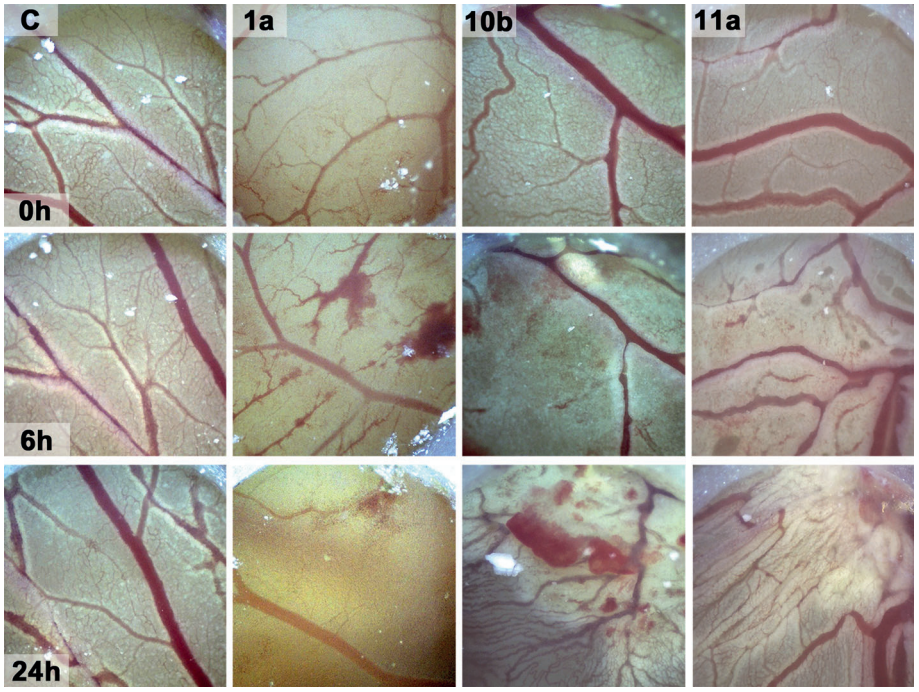

Figure 6. Effects of **1a** (10 nmol in 10 μL H_2O) and the most active complexes **10b** and **11a** (each 2.5 nmol in 10 μL H_2O) on vascularization of the chorioallantoic membrane of fertilized chicken eggs after 6 and 24 h. C: control (DMF); images are representative of three independent assays.

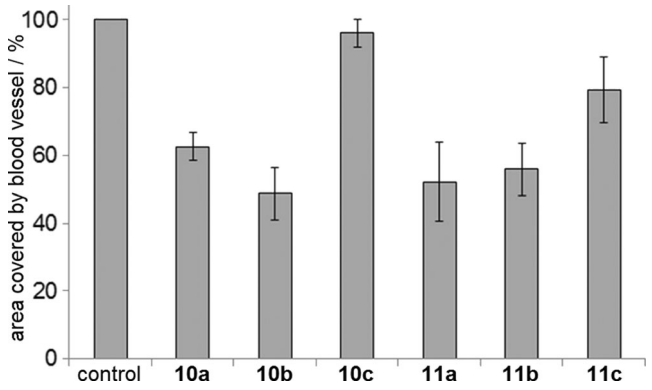

Figure 7. Vessel area analysis (derived from fractal analysis) after 6 h incubation with complexes **10** and **11** (each 2.5 nmol in 10 μL H_2O). The area in the image sections covered by blood vessels before treatment with the complexes (0 h) was set at 100%. Values are the means ± SD of three vessel area analysis calculations.

Mouse xenograft model

Finally, we evaluated the in vivo antitumor activity and tolerance of gold complexes **11a** and **11c** in a Balb/c mouse xenograft model of highly metastatic B16-F10 mouse melanoma cells (Figure 8). Fourteen days after subcutaneous implantation of 200000 cells the mice were repeatedly administered complex **11a** or **11c** at 15 mg (kg body weight)$^{-1}$ on two consecutive days. This treatment was tolerated well by the mice, merely resulting in a slight and reversible decrease in body weight, but noticeable tumor regression, as depicted in Figure 8. For both test compounds slight tumor regrowth could be detected a few days after the first dual-dose application. However, the second dual dose of **11a** or **11c** decreased the tumor volumes further. These preliminary results are indicative of considerable in vivo antitumor activity against this type of tumor and of excellent tolerance of this compound class.

Conclusions

The new gold biscarbene complexes **10** and **11** are strongly cytotoxic with low sub-micromolar IC_{50} values against various cancer cell lines including multidrug-resistant lines and those refractory to the lead compound CA-4 (**1a**). The *N*-ethyl complexes **11** are generally more active than the *N*-methyl congeners **10**. Notably, Gust and co-workers[43] reported comparably high cytotoxicities against three cancer lines for analogous *N*-ethyl biscarbene gold complexes bearing four indentical *para*-methoxy, -hydroxy, or -fluoro substituted phenyl rings.

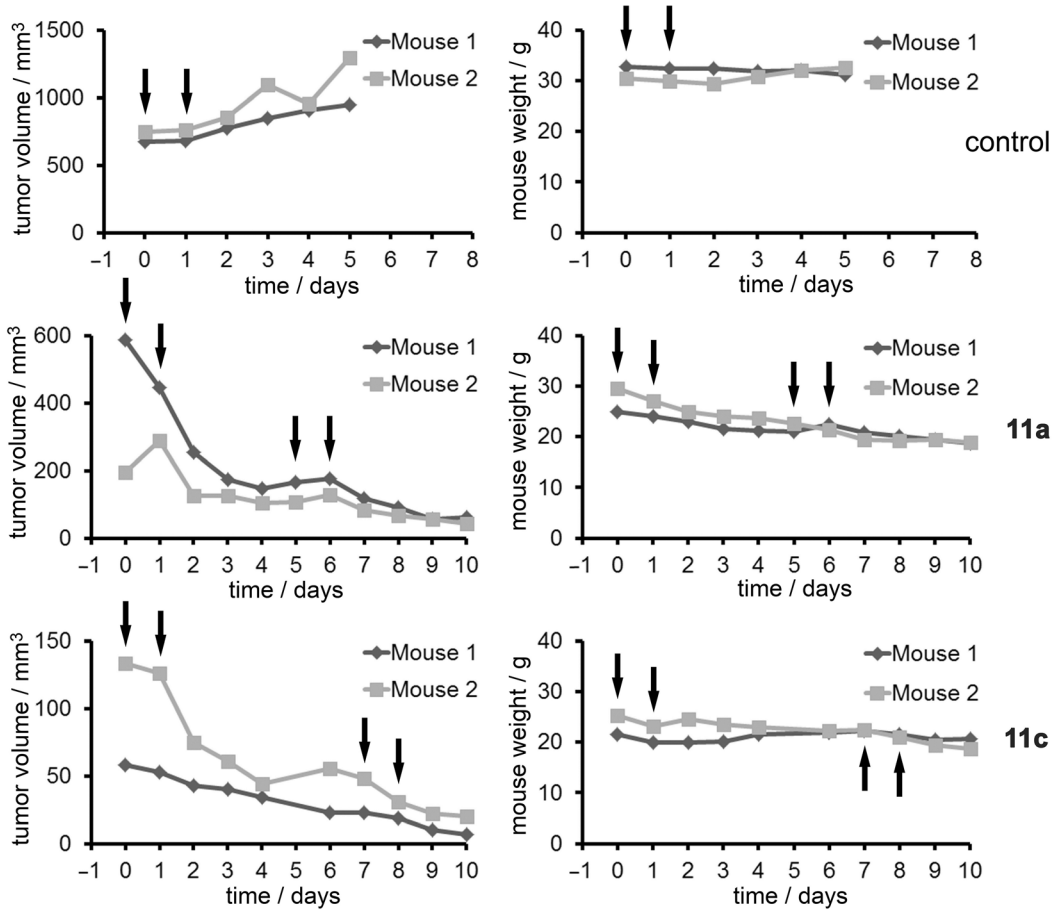

Figure 8. In vivo effects of **11a** and **11c** in mouse xenografts of the highly metastatic B16-F10 melanoma cell line. Shown are the tumor responses following single (control) and repeated (complexes **11a** and **11c**) dual-dose applications. Arrows indicate the administration of test compounds or vehicle control (DMSO).

While unable to pinpoint their mode of action, they could exclude thioredoxin reductase, estrogen receptor and cyclooxygenase (COX) as potential targets. In the case of complexes **10** and **11**, the residue R^1 seems to be decisive for cell line specificity. The all-methoxy substituted complexes **10a** and **11a** are most active against HT-29 colon carcinoma cells, which are tumorigenic and when implanted in mice form slowly growing, poorly vascularized tumors. Therefore, in this case, the greater cytotoxicity compensates for the less pronounced antivascular effect of the drug. All complexes **10** and **11** exhibit distinct vascular-disrupting effects in vitro and in vivo, resembling those effected by lead **1a** in magnitude and morphology, yet originating from a different mode of action. Whereas **1a** targets the microtubules of cancer and endothelial cells causing a G_2/M cell-cycle arrest, complexes **10** and **11** interfere only with the F-actin dynamics by stress fiber formation, leading to G_1 phase arrest. As a consequence, cell motility is severely impaired. This contributes to the overall antimetastatic effect of **10** and **11** which is further enhanced by the decrease in the concentration of prometastatic MMP-2 expressed and secreted by cancer cells. A similar effect has not been observed for the lead compound **1a**.

Apart from their unique and multimodal mechanism of action, two more clinically relevant aspects render **10** and **11** superior to **1a** and thus as promising candidates for further investigation and development: first, their strong impact on mouse xenografts of a highly metastatic melanoma cell line and the possibility to administer the compounds repeatedly and at high doses, as they are very well tolerated by the animals; second, the fact that the chorioallantoic membrane of hen eggs, after eradication of vasculature by complexes **10** and **11**, was able to recover and sprout new blood vessels might provide a tool for the new concept of "normalization of tumor vasculature",[44] that is, the replacement of irregular tumor blood vessels with normal vessels, allowing a better perfusion of the tumor with conventional anticancer drugs. At this point, we also wish to identify similarities in the modes of action between our new gold carbene complexes and NAMI-A,[45] the most advanced antimetastatic metallodrug candidate that also features an ionic imidazole transition metal complex.

Experimental Section

Column chromatography: silica gel 60 (230–400 mesh). Melting points (uncorrected), Electrothermal 9100; IR spectra, PerkinElmer Spectrum One FT-IR spectrophotometer with ATR sampling unit; NMR spectra, Bruker Avance 300 spectrometer, chemical shifts (δ) are given in ppm downfield from tetramethylsilane as internal standard; Mass spectra, Thermo Finnigan MAT 8500 (EI), Waters UPLC-Q-TOF (ESI, for HRMS). All tested compounds were $>98\%$ pure, as determined by high-resolution mass spectrometry and HPLC analysis. All starting compounds were purchased from the usual retailers and used without further purification.

Chemistry

Bis[4-(4-methoxyphenyl)-5-(3,4,5-trimethoxyphenyl)-1,3-dimethylimidazol-2-ylidene]gold(I) tetrafluoroborate (10a): A solution of imidazolium salt **8a** (22 mg, 0.048 mmol) in CH_2Cl_2/MeOH (1:1, 30 mL) was treated with Ag_2O (13 mg, 0.056 mmol) and stirred in the dark at room temperature for 5 h. $AuCl(Me_2S)$ (9 mg, 0.03 mmol) was added, and the reaction mixture was stirred for another 20 h. The suspension was filtered, the filtrate was concentrated in vacuum, and the residue was re-dissolved in CH_2Cl_2 and filtered over $MgSO_4$/Celite. The filtrate was concentrated in vacuum, and the residue dried in vacuum. Yield: 20 mg (82%); colorless solid; mp: 108 °C; ^{1}H NMR (300 MHz, $CDCl_3$): $\delta=3.72$ (s, 12H, 4× Me), 3.79 (s, 12H, 4×Me), 3.82 (s, 6H, 2×Me), 3.88 (s, 6H, 2×Me), 6.40 (s, 4H, $2\times C_6H_2(OMe)_3$), 6.88 (d, $J=8.8$ Hz, 4H, $2\times C_6H^{meta}{}_2H^{ortho}{}_2(OMe)$), 7.15 ppm (d, $J=8.8$ Hz, 4H, $2\times C_6H^{meta}{}_2H^{ortho}{}_2(OMe)$); ^{13}C NMR (75.5 MHz, $CDCl_3$): $\delta=36.4$ (NMe), 36.7 (NMe), 55.3 (OMe), 56.2 (OMe), 60.9 (OMe), 107.7, 114.4, 119.4, 122.7, 132.2, 138.7, 153.4, 160.3 ppm (NCCN), 183.6 (AuC); ^{11}B NMR (96.3 MHz, $CDCl_3$): $\delta=-3.45$ ppm; IR (ATR): $\tilde{\nu}_{max}=2935$, 2836, 1607, 1580, 1517, 1503, 1458, 1410, 1357, 1315, 1292, 1247, 1178, 1123, 1052, 1004, 1021, 909, 837, 818, 789, 765, 732, 670 cm^{-1}; MS (EI, 70 eV): *m/z* (%): 565 (4), 368 (100), 353 (92), 338 (54), 298 (96), 283 (84), 221 (88), 149 (24); HRMS (ESI): *m/z* (%): calcd: 935.3205, 934.3171, 933.3138; found: 935.3234 (16), 934.3167 (58), 933.3072 (100) $[C_{42}H_{48}AuN_4O_8{}^+]$; Anal. calcd for $C_{42}H_{48}AuBF_4N_4O_8$: C 49.43, H 4.74, N 5.49, found: C 49.58, H 4.69, N 5.39.

Bis[4-(4-methoxyphenyl)-5-(3-chloro-4,5-dimethoxyphenyl)-1,3-dimethylimidazol-2-ylidene]gold(I) tetrafluoroborate (10b): Analogously to the synthesis of **10a**, complex **10b** (42 mg, 81%) was obtained from **8b** (46 mg, 0.101 mmol), Ag_2O (27 mg, 0.116 mmol), and $AuCl(Me_2S)$ (19 mg, 0.063 mmol) as an off-white solid; mp: 130 °C; ^{1}H NMR (300 MHz, $CDCl_3$): $\delta=3.77$ (s, 6H, 2×Me), 3.82 (s, 6H, 2×Me), 3.84 (s, 6H, 2×Me), 3.89 (s, 12H, 4×Me), 6.71 (s, 2H, 2×CHCCl), 6.84 (s, 2H, CHCCCCl), 6.94 (d, $J=8.8$ Hz, 4H, $2\times C_6H^{meta}{}_2H^{ortho}{}_2(OMe)$), 7.18 ppm (d, $J=8.8$ Hz, 4H, $2\times C_6H^{meta}{}_2H^{ortho}{}_2(OMe)$); ^{13}C NMR (75.5 MHz, $CDCl_3$): $\delta=36.4$ (NMe), 36.6 (NMe), 55.3 (OMe), 56.2 (OMe), 60.7 (OMe), 113.4, 114.5, 118.9, 123.5, 123.7, 128.4, 130.8, 131.7, 132.5, 146.1, 153.9, 160.4 NCCN), 183.8 ppm (AuC); ^{11}B NMR (96.3 MHz, $CDCl_3$) $\delta=-1.70$ ppm; IR (ATR): $\tilde{\nu}_{max}=$ 2952, 2031, 1561, 1515, 1492, 1455, 1404, 1293, 1251, 1177, 1032, 915, 834, 758, 710 cm^{-1}; MS (EI, 70 eV): *m/z* (%): 568 (3), 535 (3), 421 (9), 372 (100), 302 (45); HRMS (ESI): *m/z* (%): calcd: 941.2154, 943.2130, 944.2158; found: 941.2202 (100) $[C_{40}H_{42}AuCl_2N_4O_6{}^+]$, 943.2221 (69), 944.2181 (35).

Bis[4-(4-methoxyphenyl)-5-(3-bromo-4,5-dimethoxyphenyl)-1,3-dimethylimidazol-2-ylidene]gold(I) tetrafluoroborate (10c): Analogously to the synthesis of **10a**, complex **10c** (30 mg, 80%) was obtained from **8c** (34 mg, 0.067 mmol), Ag_2O (18 mg, 0.077 mmol), and $AuCl(Me_2S)$ (12 mg, 0.041 mmol) as an off-white solid; mp: 132 °C; ^{1}H NMR (300 MHz, $CDCl_3$): $\delta=3.77$ (s, 6H, 2×Me), 3.83 (s, 6H, 2×Me), 3.84 (s, 6H, 2×Me), 3.89 (s, 6H, 2×Me), 3.90 (s, 6H, 2× Me), 6.76 (s, 2H, 2×CHCCCBr), 6.94 (d, $J=8.8$ Hz, 4H, $2\times C_6H^{meta}{}_2H^{ortho}{}_2(OMe)$), 7.00 (s, 2H, 2×CHCBr), 7.19 ppm (d, $J=8.8$ Hz, 4H, $2\times C_6H^{meta}{}_2H^{ortho}{}_2(OMe)$); ^{13}C NMR (75.5 MHz, $CDCl_3$): $\delta=36.4$ (NMe), 36.6 (NMe), 55.3 (OMe), 56.2 (OMe), 60.6 (OMe), 114.1, 114.5, 117.7, 119.0, 124.3, 126.2, 130.6, 131.7, 132.5, 153.7, 160.4 (NCCN), 183.8 ppm (AuC); ^{11}B NMR (96.3 MHz, $CDCl_3$) $\delta=-1.29$ ppm; IR (ATR): $\tilde{\nu}_{max}=2924$, 2853, 1606, 1589, 1554, 1515, 1489, 1461, 1427, 1404, 1292, 1250, 1177, 1020, 914, 830, 808, 788, 754, 737, 702, 665 cm^{-1}; MS (EI, 70 eV): *m/z* (%): 613 (2), 468 (10), 419 (100), 348 (85), 331 (40), 148 (100); HRMS (ESI): *m/z* (%): calcd: 1029.1143, 1031.1127, 1033.1106; found: 1029.1241 (52), 1031.1227 (100) $[C_{40}H_{42}AuBr_2N_4O_6{}^+]$, 1033.1233 (64).

Bis[4-(4-methoxyphenyl)-5-(3,4,5-trimethoxyphenyl)-1,3-diethyl imidazol-2-ylidene]gold(I) tetrafluoroborate (11a): Analogously

to the synthesis of **10a**, complex **11a** (100 mg, 40%) was obtained from **9a** (110 mg, 0.23 mmol), Ag_2O (61 mg, 0.26 mmol), and AuCl(Me_2S) (42 mg, 0.14 mmol) as an off-white solid; mp: 102–105 °C; ^{1}H NMR (300 MHz, $CDCl_3$): δ = 1.37 (t, J = 7.2 Hz, 6H, 2×Me), 1.43 (t, J = 7.2 Hz, 6H, 2×Me), 3.72 (s, 12H, 4×OMe), 3.77 (s, 6H, 2×OMe), 3.81 (s, 6H, 2×OMe), 4.17 (q, J = 7.2 Hz, 4H, 2×CH_2), 4.27 (q, J = 7.2 Hz, 4H, 2×CH_2), 6.40 (s, 4H, 2×C_6H_2(OMe)$_3$), 6.88 (d, J = 8.7 Hz, 4H, 2×$C_6H^{meta}{}_2H^{ortho}{}_2$(OMe)), 7.16 ppm (d, J = 8.7 Hz, 4H, 2×$C_6H^{meta}{}_2H^{ortho}{}_2$(OMe)); ^{13}C NMR (75.5 MHz, $CDCl_3$): δ = 17.3 (Me), 17.6 (Me), 44.1 (CH_2), 44.3 (CH_2), 55.3 (OMe), 56.2 (OMe), 60.8 (OMe), 107.7, 114.4, 119.3, 122.7, 131.5, 131.6, 131.8, 138.7, 153.3, 160.3 (NCCN), 182.2 ppm (AuC); ^{11}B NMR (96.3 MHz, $CDCl_3$) δ = −0.92 ppm; IR (ATR): $\tilde{\nu}_{max}$ = 2933, 2837, 1607, 1580, 1514, 1503, 1460, 1412, 1349, 1330, 1291, 1239, 1177, 1123, 1050, 1024, 1006, 886, 838, 810, 745, 731, 667 cm^{-1}; HRMS (ESI): *m/z* (%): calcd: 991.3831, 990.3797, 989.3764; found: 991.3827 (20), 990.3737 (56), 989.3652 (100) [$C_{46}H_{56}AuN_4O_8^+$]; Anal. calcd for $C_{46}H_{56}AuBF_4N_4O_8$: C 51.31, H 5.24, N 5.20, found: C 51.21, H 5.12, N 5.07.

Bis[4-(4-methoxyphenyl)-5-(3-chloro-4,5-dimethoxyphenyl)-1,3-diethylimidazol-2-ylidene]gold(I) tetrafluoroborate (11b): Analogously to the synthesis of **10a**, complex **11b** (25 mg, 75%) was obtained from **9b** (30 mg, 0.061 mmol), Ag_2O (16 mg, 0.071 mmol), and AuCl(Me_2S) (12 mg, 0.04 mmol) as an off-white solid; mp: 94 °C; ^{1}H NMR (300 MHz, $CDCl_3$): δ = 1.31–1.47 (m, 12H, 4×Me), 3.73–3.79 (m, 6H, 2×OMe), 3.80–3.84 (m, 6H, 2×OMe), 3.85–3.89 (m, 6H, 2×OMe), 4.13–4.37 (m, 8H, 4×CH_2), 6.63–6.77 (m, 2H, 2×CHCCCl), 6.81–6.87 (m, 2H, 2×CHCCl), 6.88–6.99 (m, 4H, 2×$C_6H^{meta}{}_2H^{ortho}{}_2$(OMe)), 7.13–7.22 ppm (m, 4H, 2×$C_6H^{meta}{}_2H^{ortho}{}_2$-(OMe)); ^{13}C NMR (75.5 MHz, $CDCl_3$): δ = 16.8 (Me), 17.0 (Me), 17.3 (Me), 17.5 (Me), 44.2 (CH_2), 44.4 (CH_2), 55.3 (OMe), 56.3 (OMe), 60.7 (OMe), 113.5, 114.4, 114.5, 118.9, 123.6, 123.7, 124.6, 128.4, 130.3, 131.7, 131.9, 132.0, 146.0, 146.2, 153.8, 153.9, 160.3, 160.5 (NCCN), 182.5 ppm (AuC); ^{11}B NMR (96.3 MHz, $CDCl_3$) δ = −1.28 ppm; IR (ATR): $\tilde{\nu}_{max}$ = 2933, 1606, 1562, 1514, 1491, 1461, 1409, 1345, 1319, 1292, 1250, 1176, 1158, 1110, 1090 1040, 1032, 997, 899, 835, 811, 756 cm^{-1}; MS (EI, 70 eV): *m/z* (%): 597 (3), 416 (11), 372 (100), 357 (75); HRMS (ESI): *m/z* (%): calcd: 997.2773, 999.2772, 1000.2793; found: 997.2779 (100) [$C_{44}H_{50}AuCl_2N_4O_6^+$], 999.2802 (77), 1000.2938 (35).

Bis[4-(4-methoxyphenyl)-5-(3-bromo-4,5-dimethoxyphenyl)-1,3-diethylimidazol-2-ylidene]gold(I) tetrafluoroborate (11c): Analogously to the synthesis of **10a**, complex **11c** (35 mg, 77%) was obtained from **9c** (41 mg, 0.077 mmol), Ag_2O (21 mg, 0.089 mmol), and AuCl(Me_2S) (14 mg, 0.048 mmol) as an off-white solid; mp: 104 °C; ^{1}H NMR (300 MHz, $CDCl_3$): δ = 1.43 (m, 12H, 4×Me), 3.79 (s, 6H, 2×OMe), 3.83–3.90 (m, 12H, 4×OMe), 4.18–4.34 (m, 8H, 4×CH_2), 6.79 (s, 2H, 2×CHCCCBr), 6.95 (d, J = 8.9 Hz, 4H, 2×$C_6H^{meta}{}_2H^{ortho}{}_2$(OMe)), 7.03 (s, 2H, 2×CHCBr), 7.21 ppm (d, J = 8.9 Hz, 4H, 2×$C_6H^{meta}{}_2H^{ortho}{}_2$(OMe)); ^{13}C NMR (75.5 MHz, $CDCl_3$): δ = 16.8 (Me), 17.1 (Me), 17.3 (Me), 44.2 (CH_2), 44.3 (CH_2), 44.4 (CH_2), 55.3 (OMe), 56.1 (OMe), 56.3 (OMe), 60.5 (OMe), 114.2, 114.5, 117.6, 119.0, 124.4, 126.3, 130.1, 130.2, 131.7, 131.9, 131.9, 153.8, 160.4 (NCCN), 182.5 ppm (AuC); ^{11}B NMR (96.3 MHz, $CDCl_3$) δ = −1.67 ppm; IR (ATR): $\tilde{\nu}_{max}$ = 3435, 2981, 2937, 2192, 1606, 1588, 1554, 1515, 1489, 1462, 1418, 1398, 1351, 1293, 1251, 1176, 1150, 1076, 1026, 995, 918, 894, 840, 806, 776, 726 cm^{-1}; MS (EI, 70 eV): *m/z* (%): 719 (9), 642 (15), 563 (6), 458 (60); HRMS (ESI): *m/z* (%): calcd: 1085.1773, 1087.1765, 1089.1730; found: 1085.1842 (55), 1087.2778 (100) [$C_{44}H_{50}AuCl_2N_4O_6^+$], 1089.1682 (70).

Biology

Cell lines and culture conditions: The human melanoma cell line 518A2 was obtained from the Department of Radiotherapy, Medical University of Vienna (Austria). The KB-V1/Vbl and MCF-7/Topo cell lines were obtained from the Institute of Pharmacy at the University Regensburg (Germany), and the HCT-116 colon and Panc-1 pancreatic carcinoma cell lines from the University Hospital Erlangen (Germany). The human HT-29 colon carcinoma cell line (ACC-581) was purchased from the German Centre of Biological Materials (DSMZ), Braunschweig, Germany. Human umbilical vein endothelial cells (HUVEC) were provided by the Helmholtz Center for Infection Research, Braunschweig. All cell lines were grown at 37 °C, 5% CO_2, 95% humidity in Dulbecco's modified Eagle's medium (DMEM) containing 10% fetal bovine serum (FBS), 1% antibiotic–antimycotic, and 250 μg mL^{-1} gentamycin (all from Gibco), apart from HT-29 cells, which were grown in RPMI-1640 medium (10% FBS, 1% antibiotic–antimycotic, 250 μg mL^{-1} gentamycin) and HUVEC, which were cultured in EGM-2 medium (Lonza) supplemented with 5% FBS. Only mycoplasma-free cultures were used.

Determination of tumor cell growth: 3-(4,5-Dimethylthiazol-2-yl)-2,5-diphenyltetrazolium bromide (MTT; ABCR) was used to identify viable cells that reduce it to a violet formazan.[21] See the Supporting Information for a detailed description.

Fluorescence labeling of actin filaments: Effects of **1a** and complexes **10** and **11** on the organization of F-actin in HUVEC and 518A2 melanoma cells were examined by fluorescence microscopy. Cells were cultured on glass coverslips to 75% confluence. For HUVEC the glass coverslips were pretreated with 1 M HCl/EtOH. Following treatment with **1a**, **10**, or **11** (for HUVEC: 100 nM **1a**; 100, 500 nM and 1 μM **10** or **11**; for 518A2 cells: 2.5 nM **1a**; 250 and 500 nM of **10** or **11**) or vehicle for 24 h, cells were fixed with 3.5% formalin (in PBS) for 10 min, washed with PBS and permeabilized with 0.1% Triton X-100 (5 min). Then cells were washed and F-actin was stained (37 °C, 1 h) using Alexa Fluor 488 Phalloidin (Invitrogen) 1:100. Nuclei were counterstained with DAPI (1 μg mL^{-1} in PBS, room temperature, 5 min) before coverslips were washed in PBS and mounted with ProLong Gold Antifade reagent (Invitrogen). Effects were analyzed using an Axioplan fluorescence microscope with a 40× objective lens (Zeiss, AxioCam MRm).

Cell-cycle analysis: 518A2 cells (5×10^4 mL) were grown on six-well plates for 24 h and then treated with 5 nM **1a** and 500 of **10** or **11** for 24 h. Solvent controls (DMSO or DMF) were treated identically. After fixation (70% EtOH, 4 °C) the cells were incubated with propidium iodide (PI; Roth) staining solution (50 μg mL^{-1} PI, 0.1% sodium citrate, 50 μg mL^{-1} RNase A in PBS) for 30 min at 37 °C. The fluorescence intensity of 10000 single cells was measured at λ_{em} = 620 nm (λ_{ex} = 488 nm laser source) using a Beckman Coulter Cytomics FC 500 flow cytometer and analyzed (CXP Analysis, Beckman Coulter) for the fractions of cells in G_1, S, and G_2/M phase. The percentage of apoptotic cells was assessed from sub-G_1 peaks.

Wound-healing assay: 518A2 melanoma cells (1×10^5 mL) were seeded on 24-well plates and grown to a sub-confluent monolayer. A narrow artificial wound was created by scraping off a strip of cells with a 20–200 μL plastic tip. The medium was replaced before cells were treated with 5 nM **1a**, 500 nM **10** or **11**, or vehicle (DMF) for up to 48 h. The wound-healing process was monitored microscopically (Axiovert 135 with a 10× objective lens, Zeiss, AxioCam MRc5) after 24 and 48 h exposure to test compounds. Wound size was measured at three different positions (top, middle, bottom) of each microscopy image using Adobe Photoshop CS6 (version 13.01). Thereby, the mean width of the wound was calculated for

each documented time point (0, 24, and 48 h), and the percentage of wound healing over time was determined.

Gelatin zymography: 518A2 cells (1×10^5 mL) were seeded on six-well plates and cultured for 24 h. After replacement of the medium with fresh DMEM supplemented with 0.1% BSA (Roth) and 200 (kIU aprotinin) mL^{-1} (AppliChem), complexes **10** and **11** were added (dilution series of 10 mM stock solutions in DMF ranging from 0.1 to 2.5 μM in H_2O), and incubation was continued for a further 24 h. For solvent controls respective amounts of DMF were applied. Both the preparation of conditioned media and cell lysates as well as the gelatin zymography itself were carried out according to published methods.[46] Samples used for gelatin zymography were normalized to protein concentration (for each sample 20 μg total protein were applied to the gels).

Chorioallantoic membrane (CAM) assay: Fertilized, specific pathogen-free (SPF) chicken eggs (VALO BioMedia) were bred in an incubator at 37 °C and 60% relative humidity. On day 5 windows (Ø 1.5–2 cm) were cut into the eggshell at the more rounded pole. The cavities were sealed with tape, and incubation was continued for 12–18 h. Then rings of thin silicon foil (Ø 5 mm) were placed on the CAM with its developing blood vessels, and **1a** (10 nmol), **10** or **11** (2.5 nmol) or respective amounts of DMSO or DMF as solvent controls (all in a volume of 10 μL H_2O) were added. The effects on the developing vasculature were documented after further incubation for 6 and 24 h using a light microscope (60× magnification, Traveler).[39,40] For quantitative evaluation, image sections were taken from the light microscopy pictures and the area taken up by blood vessels (fractal dimension) was determined by fractal analysis[41,42] using the following software: ImageJ 1.48f and Fractal Analysis System 3.4.7 (see the Supporting Information for a detailed description). The area in the image sections covered by blood vessels (fractal dimension) before treatment with the test compounds was set at 100%, and the decrease in this area after exposure to gold complexes **10** and **11** for 6 h was determined.

Animal studies: All animal work was approved by the committee on animal care (Government of Rhineland Palatinate). The mice (Balb/c) were kept under a 12 h light–dark cycle in a controlled conventional colony room. The mice had free access to sterilized water and standard rodent diet ad libitum. The mice were sacrificed by cervical dislocation corresponding to the guidelines of the committee on animal care. To analyze the in vivo antitumor activity and tolerance of gold complexes **11a** and **11c**, a Balb/c mouse xenograft model of highly metastatic B16-F10 mouse melanoma cells (Department of Dermatology, Medical University Mainz, Germany) was used. A suspension of 2×10^5 cells in 200 μL PBS was administered to the flanks of each mouse to generate subcutaneous xenograft tumors. For these in vivo studies, the gold complexes **11a** and **11c** were dissolved in DMSO and further diluted with PBS. The mice ($n=2$) were injected i.p. with 15 mg (kg body weight)$^{-1}$ of complex **11a** or **11c** twice on two consecutive days. Control mice ($n=2$) were treated with respective amounts of DMSO (in PBS) only once on two consecutive days. The size of the tumors and the weight of the mice were recorded on a daily basis beginning on the day of the first injection. Tumor volumes were calculated by the formula $a^2 \cdot b \cdot 0.5$, with a being the short dimension and b the long dimension.

Acknowledgements

We thank the COST Action CM1105 "Functional metal complexes that bind to biomolecules" and the Deutsche Forschungsgemeinschaft (grant Scho 402/8-3) for financial support, Dr. Thomas Mueller (Department of Internal Medicine IV, Oncology/Hematology, Martin Luther University, Halle-Wittenberg) for tubulin polymerization assays, Dr. Holger Schmidt (Department of Plant Physiology, University Bayreuth) for high-resolution mass spectra, and the Elite Study Program "Macromolecular Science", Elite Network of Bavaria, for its support (J.K.M.).

Keywords: antimetastatic agents · carbene ligands · gold · matrix metalloproteinases · vascular-disrupting agents

[1] G. Taraboletti, B. Margosio, *Curr. Opin. Pharmacol.* **2006**, *1*, 378 – 384.
[2] J. W. Lippert III, *Bioorg. Med. Chem.* **2007**, *15*, 605 – 615.
[3] S. M. Weis, D. A. Cheresh, *Nat. Med.* **2011**, *17*, 1359 – 1370.
[4] D. W. Siemann, *Cancer Treat. Rev.* **2011**, *37*, 63 – 74.
[5] G. R. Pettit, S. B. Singh, E. Hamel, C. M. Lin, D. S. Alberts, D. Garcia-Kendall, *Experientia* **1989**, *45*, 209 – 211.
[6] G. M. Tozer, V. E. Prise, J. Wilson, M. Cemazar, S. Shan, M. W. Dewhirst, P. R. Barber, B. Vojnovic, D. J. Chaplin, *Cancer Res.* **2001**, *61*, 6413 – 6422.
[7] G. C. Tron, T. Pirali, G. Sorba, F. Pagliai, S. Busacca, A. A. Genazzani, *J. Med. Chem.* **2006**, *49*, 3033 – 3044.
[8] L. Vincent, P. Kermani, L. M. Young, J. Cheng, F. Zhang, K. Shido, G. Lam, H. Bompais-Vincent, Z. Zhu, D. J. Hicklin, P. Bohlen, D. J. Chaplin, C. May, S. Rafii, *J. Clin. Invest.* **2005**, *115*, 2992 – 3006.
[9] C. J. Mooney, G. Nagaiah, P. Fu, J. K. Wasman, M. M. Cooney, P. S. Savvides, J. A. Bokar, A. Dowlati, D. Wang, S. S. Agarwala, S. M. Flick, P. H. Hartman, J. D. Ortiz, P. N. Lavertu, S. C. Remick, *Thyroid* **2009**, *19*, 233 – 240.
[10] G. J. Rustin, G. Shreeves, P. D. Nathan, A. Gaja, T. S. Ganesan, D. Wang, J. Boxall, L. Poupard, D. J. Chaplin, M. R. L. Stratford, J. Balkissoon, M. Zweifel, *Br. J. Cancer* **2010**, *102*, 1355 – 1360.
[11] P. D. Nathan, M. Zweifel, A. R. Padhani, D. M. Koh, M. Ng, D. J. Collins, A. Harris, C. Carden, J. Smythe, N. Fisher, N. J. Taylor, J. J. Stirling, S. P. Lu, M. O. Leach, G. J. Rustin, I. Judson, *Clin. Cancer Res.* **2012**, *18*, 3428 – 3439.
[12] G. R. Pettit, M. R. Rhodes, D. L. Herald, D. J. Chaplin, M. R. L. Stratford, E. Hamel, R. K. Pettit, J.-C. Chapuis, D. Oliva, *Anti-Cancer Drug Des.* **1998**, *13*, 981 – 993.
[13] G. R. Pettit, B. E. Toki, D. L. Herald, M. R. Boyd, E. Hamel, R. K. Pettit, J.-C. Chapuis, *J. Med. Chem.* **1999**, *42*, 1459 – 1465.
[14] L. Wang, K. W. Woods, Q. Li, K. J. Barr, R. W. McCroskey, S. M. Hannick, L. Gherke, R. B. Credo, Y.-H. Hui, K. Marsh, R. Warner, J. Y. Lee, N. Zielinski-Mozng, D. Frost, S. H. Rosenberg, H. L. Sham, *J. Med. Chem.* **2002**, *45*, 1697 – 1711.
[15] T. Brown, H. Holt, Jr., M. Lee in *Heterocyclic Antitumor Antibiotics* (Ed.: M. Lee), Springer, Berlin/Heidelberg, **2006**, pp. 1 – 51.
[16] R. Schobert, B. Biersack, A. Dietrich, K. Effenberger, S. Knauer, T. Müller, *J. Med. Chem.* **2010**, *53*, 6595 – 6602.
[17] W. Liu, R. Gust, *Chem. Soc. Rev.* **2013**, *42*, 755 – 773.
[18] L. Oehninger, R. Rubbiani, I. Ott, *Dalton Trans.* **2013**, *42*, 3269 – 3284.
[19] L. Kaps, B. Biersack, H. Müller-Bunz, K. Mahal, J. Muenzner, M. Tacke, T. Mueller, R. Schobert, *J. Inorg. Biochem.* **2012**, *106*, 52 – 58.
[20] J. Münzner, B. Biersack, L. Kaps, R. Schobert, F. Sasse, *Int. J. Clin. Pharmacol. Ther.* **2013**, *51*, 44 – 46.
[21] T. Mosmann, *J. Immunol. Methods* **1983**, *65*, 55 – 63.
[22] D. W. Shen, C. Cardarelli, J. Hwang, M. Cornwell, N. Richert, S. Ishii, I. Pastan, M. M. Gottesman, *J. Biol. Chem.* **1986**, *261*, 7762 – 7770.
[23] M. M. Cornwell, A. R. Safa, R. L. Felsted, M. M. Gottesman, I. Pastan, *Proc. Natl. Acad. Sci. USA* **1986**, *83*, 3847 – 3850.
[24] A. Fojo, S. Akiyama, M. M. Gottesman, I. Pastan, *Cancer Res.* **1985**, *45*, 3002 – 3007.
[25] M. C. Willingham, M. M. Cornwell, C. O. Cardarelli, M. M. Gottesman, I. Pastan, *Cancer Res.* **1986**, *46*, 5941 – 5946.
[26] S. K. Rabindran, D. D. Ross, L. A. Doyle, W. Yang, L. M. Greenberger, *Cancer Res.* **2000**, *60*, 47 – 50.
[27] C. Hirschmann-Jax, A. E. Foster, J. G. Nuchtern, T. W. Jax, U. Gobel, M. A. Goodell, M. K. Brenner, *Proc. Natl. Acad. Sci. USA* **2004**, *101*, 14228 – 14233.

[28] C. Kanthou, G. M. Tozer, *Blood* **2002**, *99*, 2060 – 2069.
[29] J. Huot, F. Houle, S. Rousseau, R. G. Deschesnes, G. M. Shah, J. Landry, *J. Cell Biol.* **1998**, *143*, 1361 – 1373.
[30] H. Y. Yamada, G. J. Gorbsky, *Mol. Cancer Ther.* **2006**, *5*, 2963 – 2969.
[31] H. L. Lin, S. H. Chiou, C. W. Wu, W. B. Lin, L. H. Chen, Y. P. Yang, M. L. Tsai, Y. H. Uen, J. P. Liou, C. W. Chi, *J. Pharmacol. Exp. Ther.* **2007**, *323*, 365 – 373.
[32] E. A. Papakonstanti, C. Stournaras, *FEBS Lett.* **2008**, *582*, 2120 – 2127.
[33] S. Pellegrin, H. Mellor, *J. Cell Sci.* **2007**, *120*, 3491 – 3499.
[34] C. Gialeli, A. D. Theocharis, N. K. Karamanos, *FEBS J.* **2011**, *278*, 16 – 27.
[35] U. B. Hofmann, J. R. Westphal, G. N. Van Muijen, D. J. Ruiter, *J. Invest. Dermatol.* **2000**, *115*, 337 – 344.
[36] P. A. Snoek-van Beurden, J. W. Von den Hoff, *Biotechniques* **2005**, *38*, 73 – 83.
[37] M. L. Ponce, *Methods Mol. Biol.* **2009**, *467*, 183 – 188.
[38] Y. Muthukumar, M. Roy, A. Raja, R. E. Taylor, F. Sasse, *ChemBioChem* **2013**, *14*, 260 – 264.
[39] K. Norrby, *J. Cell. Mol. Med.* **2006**, *10*, 588 – 612.
[40] B. Nitzsche, C. Gloesenkamp, M. Schrader, M. Ocker, R. Preissner, M. Lein, A. Zakrzewicz, B. Hoffmann, M. Höpfner, *Br. J. Cancer* **2010**, *103*, 18 – 28.
[41] L. M. Kirchner, S. P. Schmidt, B. S. Gruber, *Microvasc. Res.* **1996**, *51*, 2 – 14.
[42] B. R. Masters, *Annu. Rev. Biomed. Eng.* **2004**, *6*, 427 – 452.
[43] W. Liu, K. Bensdorf, M. Proetto, A. Hagenbach, U. Abram, R. Gust, *J. Med. Chem.* **2012**, *55*, 3713 – 3724.
[44] R. K. Jain, *Science* **2005**, *307*, 58 – 62.
[45] A. Bergamo, G. Sava, *Dalton Trans.* **2011**, *40*, 7817 – 7823.
[46] S. Rodríguez-Nieto, M. González-Iriarte, R. Carmona, R. Muñoz-Chápuli, M. A. Medina, A. R. Quesada, *FASEB J.* **2001**, *15*, 261 – 263.

Received: January 21, 2014
Published online on March 19, 2014